



Relationship between interlayer hydration and photocatalytic water splitting of $A'_{1-x}Na_xCa_2Ta_3O_{10} \cdot nH_2O$ ($A' = K$ and Li)

Tomohiro Mitsuyama, Akiko Tsutsumi, Sakiko Sato, Keita Ikeue, Masato Machida*

Department of Nano Science and Technology, Graduate School of Science and Technology, Kumamoto University, 2-39-1 Kurokami, Kumamoto 860-8555, Japan

ARTICLE INFO

Article history:

Received 22 December 2007

Received in revised form

14 March 2008

Accepted 22 March 2008

Available online 26 March 2008

Keywords:

Layered perovskite tantalate

Ion exchange

Interlayer hydration

Photocatalyst

ABSTRACT

Partial replacement of alkaline metals in anhydrous $KCa_2Ta_3O_{10}$ and $LiCa_2Ta_3O_{10}$ was studied to control interlayer hydration and photocatalytic activity for water splitting under UV irradiation. $A'_{1-x}Na_xCa_2Ta_3O_{10} \cdot nH_2O$ ($A' = K$ and Li) samples were synthesized by ion exchange of $CsCa_2Ta_3O_{10}$ in mixed molten nitrates at 400 °C. In $K_{1-x}Na_xCa_2Ta_3O_{10} \cdot nH_2O$, two phases with the orthorhombic ($C222$) and tetragonal ($I4/mmm$) structures were formed at $x \leq 0.7$ and $x \geq 0.5$, respectively. Upon replacement by Na^+ having a larger enthalpy of hydration (ΔH_h^0), the interlayer hydration occurred at $x \geq 0.3$ and the hydration number (n) was increased monotonically with an increase of x . $Li_{1-x}Na_xCa_2Ta_3O_{10} \cdot nH_2O$ showed a similar hydration behavior, but the phase was changed from $I4/mmm$ ($x < 0.5$, $n \sim 0$) via $P4/mmm$ ($x \sim 0.5$, $n \sim 1$) to $I4/mmm$ ($x \sim 1.0$, $n \sim 2$). The photocatalytic activities of these systems after loading 0.5 wt% Ni were quite different each other. $K_{1-x}Na_xCa_2Ta_3O_{10} \cdot nH_2O$ exhibited the activity increasing in consistent with n , whereas $Li_{1-x}Na_xCa_2Ta_3O_{10} \cdot nH_2O$ exhibited the activity maximum at $x = 0.77$, where the rates of H_2/O_2 evolution were nearly doubled compared with those for end-member compositions ($x = 0$ and 1).

© 2008 Elsevier Inc. All rights reserved.

1. Introduction

Tantalates having perovskite-related crystal structures show wide band gaps (~ 4 eV) and high photocatalytic activity for overall water splitting under UV irradiation [1–19]. We are especially interested in layered tantalates with Dion–Jacobson and/or Ruddlesden–Popper-type structures, because their photocatalytic activity is often sensitive to the local structure of interlayer space, which can easily be modified by ion exchange and intercalation processes. It was reported that several layered oxides, such as $K_4Nb_6O_{17}$ [4,5,11] and $K_2La_2Ti_3O_{10}$ [8,9] are highly active, because water molecules to be intercalated can be accessible to active sites responsible for the photocatalytic reaction. We have studied that the photocatalytic activity of Dion–Jacobson-type-layered perovskites, $A'Ca_2Ta_3O_{10}$ ($A' = Cs, Rb, K, Na$ and Li) [19,20], focusing on their hydration behavior. Interlayer hydration is observed for $A' = Na$ only, whereas other systems are anhydrous. The photocatalytic activity in the presence of NiO_x co-catalyst was strongly dependent on A' , increasing in the order of $Cs < Rb < K < Na < Li$. The second highest activity for $A' = Na$ seems to be susceptible to its hydrated interlayer. However, it should be noted that the Li phase exhibits the highest

activity in spite of its anhydrous structure. Because Na seems to play a key role in interlayer hydration, partial replacement of other alkali metals by Na would be of great interest in the design of active hydrated photocatalysts for overall water splitting.

In this work, we have studied the Na -substitution for two anhydrous-layered tantalates, $KCa_2Ta_3O_{10}$ and $LiCa_2Ta_3O_{10}$, to yield hydrated phases, $A'_{1-x}Na_xCa_2Ta_3O_{10} \cdot nH_2O$ ($A' = K$ and Li). In order to control the amount of water molecules to be accommodated into the interlayer, compounds with different Na content (x) were synthesized by ion exchange and were applied to photocatalytic water splitting under UV irradiation. As exchanged compounds were characterized by means of X-ray diffraction (XRD), thermal gravimetric analysis (TG), FT-IR and Raman to discuss the relationship between alkaline metal ions (A'), interlayer hydration and photocatalytic activity.

2. Experimental

The powder samples of $CsCa_2Ta_3O_{10}$ were prepared by a conventional solid-state reaction of appropriate mixture of Cs_2CO_3 , $CaCO_3$ and Ta_2O_5 at 1000 °C [19]. An excess of 50 mol% amount of Cs_2CO_3 was used to compensate the loss due to its vaporization. As obtained $CsCa_2Ta_3O_{10}$ was heated in molten nitrate ($A'NO_3$, $A' = K, Na$ and Li) at 430, 400 and 280 °C, respectively, to convert to each A' -exchanged forms. To obtain $A'_{1-x}Na_xCa_2Ta_3O_{10} \cdot nH_2O$ ($A' = Li$ and K), the Cs phase was heated

* Corresponding author. Fax: +81 96 342 3651.

E-mail address: machida@chem.kumamoto-u.ac.jp (M. Machida).

in molten mixture of $A'\text{NO}_3$ ($A' = \text{K}$ or Li) and NaNO_3 at 400°C . The temperature was determined considering melting points of nitrates, i.e., KNO_3 (333°C), NaNO_3 (308°C) and LiNO_3 (261°C). As exchanged samples were washed with distilled deionized water and dried *in vacuo* at room temperature. Ni-loaded catalysts (0.5 wt% loading) were prepared by impregnation using aqueous solution of $\text{Ni}(\text{NO}_3)_2$, followed by heating at 500°C for 2 h in a stream of O_2 and subsequently at 500°C for 2 h in H_2 . Finally, as obtained catalysts were treated at 200°C in O_2 to reoxidize the surface of Ni particles prior to use in photocatalytic reactions [1,2].

Crystal structure of as prepared samples was determined by powder XRD (Rigaku Multiflex) with monochromated $\text{CuK}\alpha$ radiation (40 kV, 20 mA). Lattice constants of each crystalline phase were calculated and corrected using MDI JADE software. Chemical composition was determined by X-ray fluorescence (XRF, Horiba MESA-500W) and an inductively coupled plasma atomic emission spectrophotometer (ICP-AES, Seiko instrument, SPS7800). For ICP-AES analysis, the solid was dissolved using 23 M HF. TG (Rigaku 8120) was performed to determine the amount of interlayer water. The sample of about 10 mg was heated in a flowing 20% O_2 in N_2 at the constant rate of $10^\circ\text{C min}^{-1}$. Diffuse reflectance spectra were recorded with a UV–vis spectrometer (Jasco V-550) to determine optical band-gap energy. FT-IR spectra of water molecules in the interlayer were measured with a Jasco FT-IR-610 spectrometer. Raman spectra were obtained on a Jasco NRS-3100 spectrometer using a 532.1 nm laser as an excitation source.

Photocatalytic reactions were carried out in an inner-irradiation-type quartz vessel connected to a closed gas-circulating system. Dispersed catalyst powders (0.20 g) in 200 mL pure water by a magnetic stirrer was photo-irradiated with a 400 W high-pressure mercury lamp. The rates of H_2 and O_2 evolution were determined using a gas chromatograph (Shimadzu GC-8A, TCD, Ar carrier, MS-5A).

3. Results and discussion

3.1. Structure and hydration of triple-layered perovskite tantalates

Three-layered tantalates, $\text{LiCa}_2\text{Ta}_3\text{O}_{10}$, $\text{NaCa}_2\text{Ta}_3\text{O}_{10}$ and $\text{KCa}_2\text{Ta}_3\text{O}_{10}$, could be obtained as single phases by ion exchange of $\text{CsCa}_2\text{Ta}_3\text{O}_{10}$. Their XRD patterns were free from reflections due to $\text{CsCa}_2\text{Ta}_3\text{O}_{10}$ and more than 99% Cs could be replaced by K, Na or Li. As reported by Toda et al. [21,22], the crystal structures of these compounds are basically composed of monovalent alkali metal ions and triple perovskite slabs described as $[\text{Ca}_2\text{Ta}_3\text{O}_{10}]^-$ stacking alternatively by electrostatic interaction (Fig. 1). The Li and Na phases belong to the space groups of tetragonal ($I4/mmm$), whereas the K phase belongs to orthorhombic ($C222$). The difference arises from slide of adjacent perovskite slab by $a/2$ along the [100] direction. As described in our previous report [19,20], the Na phase contains about 2 mol mol⁻¹ of water inside the interlayer space, whereas the other two phases are stable as anhydrous phases. As shown in Fig. 1, water molecules in the interlayer would be bound each other by hydrogen bonds forming a double layer in combination with Na [21]. The water molecules can be eliminated from the interlayer by heating above 200°C . However, fast intercalation of water vapor into a dehydrated Na phase proceeded even at room temperature to restore the hydrated phase. The hydration behavior of these layered tantalates seems to be dependent on two factors, the enthalpy of hydration (ΔH_h^0) and ionic radius (r) of alkali metal [20]. The ΔH_h^0 value decreases in the order of $\text{Li}^+(-536 \text{ kJ mol}^{-1}) > \text{Na}^+(-421 \text{ kJ mol}^{-1}) > \text{K}^+(-337 \text{ kJ mol}^{-1})$, whereas the r value and

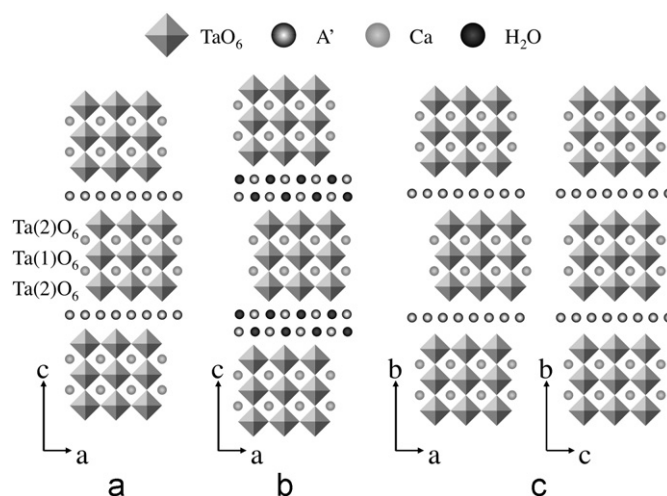


Fig. 1. Crystal structure model of (a) $\text{LiCa}_2\text{Ta}_3\text{O}_{10}$ ($I4/mmm$), (b) $\text{NaCa}_2\text{Ta}_3\text{O}_{10} \cdot 2\text{H}_2\text{O}$ ($I4/mmm$) and (c) $\text{KCa}_2\text{Ta}_3\text{O}_{10}$ ($C222$).

Table 1

Composition and structure of $\text{K}_{1-x}\text{Na}_x\text{Ca}_2\text{Ta}_3\text{O}_{10} \cdot n\text{H}_2\text{O}$

| Entry | Melt composition ^a | x | Space group | c_1/nm^b | a_1/nm^c | n^d |
|-------|-------------------------------|------|-------------|-------------------|-------------------|-------|
| a | 0 | 0 | $C222$ | 1.4863 | 0.3852 | 0 |
| b | 0.25 | 0.09 | $C222$ | 1.4854 | 0.3853 | 0 |
| c | 0.60 | 0.22 | $C222$ | 1.4769 | 0.3854 | 0 |
| d | 0.70 | 0.30 | $C222$ | 1.4706 | 0.3857 | 0.13 |
| e | 0.75 | 0.57 | $C222$ | 1.4541 | 0.3858 | 0.67 |
| f | 0.80 | 0.70 | $I4/mmm$ | 1.6882 | 0.3862 | |
| | | | $C222$ | 1.6967 | 0.3861 | 0.99 |
| g | 0.90 | 0.83 | $I4/mmm$ | 1.6956 | 0.3862 | |
| | | | $C222$ | 1.6761 | 0.3867 | 1.22 |
| h | 0.95 | 0.91 | $I4/mmm$ | 1.6907 | 0.3863 | 1.60 |
| i | 1.00 | 1.00 | $I4/mmm$ | 1.6911 | 0.3861 | 1.92 |

^a $\text{NaNO}_3/(\text{NaNO}_3+\text{KNO}_3)$.

^b d_{020} for $C222$, d_{002} for $I4/mmm$.

^c d_{001} for $C222$, $2d_{200}$ for $I4/mmm$.

^d Hydration number.

thus the interlayer distance increase in the order of $\text{Li}^+(r = 0.068 \text{ nm}) < \text{Na}^+(0.098 \text{ nm}) < \text{K}^+(0.133 \text{ nm})$. The hydration should therefore be thermodynamically favorable for the Li case, but the smallest interlayer distance would not allow water molecules to be intercalated.

3.2. $\text{K}_{1-x}\text{Na}_x\text{Ca}_2\text{Ta}_3\text{O}_{10} \cdot n\text{H}_2\text{O}$

Next, we have studied the partial replacement of K and Li by Na in the triple-layered tantalates, $A'_{1-x}\text{Na}_x\text{Ca}_2\text{Ta}_3\text{O}_{10}$ ($A' = \text{Li}$ and K), to control their hydration behavior and photocatalytic activity. $\text{K}_{1-x}\text{Na}_x\text{Ca}_2\text{Ta}_3\text{O}_{10}$ ($0 \leq x \leq 1$) was synthesized by ion exchange at 400°C using mixed molten nitrates ($\text{KNO}_3\text{--NaNO}_3$) with different ratios as shown in Table 1. The Na content (x) in the solid product was increased monotonically in accordance with the composition of mixed molten nitrates.

Fig. 2 indicates XRD pattern of as exchanged products, $\text{K}_{1-x}\text{Na}_x\text{Ca}_2\text{Ta}_3\text{O}_{10}$. Because of the different space groups of end-member compositions at $x = 0$ and 1, two different phases appeared depending on x . $\text{KCa}_2\text{Ta}_3\text{O}_{10}$ consisted of the orthorhombic lattice with the $C222$ space group ($a = 0.3865 \text{ nm}$, $b = 2.9726 \text{ nm}$ and $c = 0.3852 \text{ nm}$). Upon Na-substitution the original structure ($C222$) was retained up to $x = 0.30$, but further substitution yielded less intense ($0k0$) peaks and simultaneous appearance of peaks at lower 2θ . This can be attributed to the

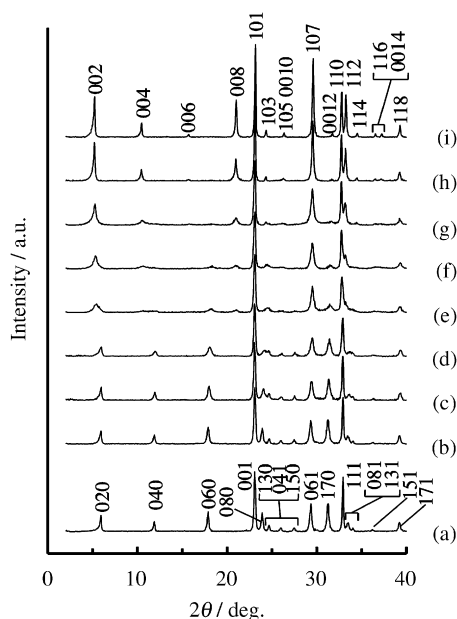


Fig. 2. XRD patterns of $K_{1-x}Na_xCa_2Ta_3O_{10} \cdot nH_2O$: (a) $x = 0$, (b) 0.09, (c) 0.22, (d) 0.30, (e) 0.57, (f) 0.70, (g) 0.83, (h) 0.91 and (i) 1.

change to the tetragonal lattice with the $I4/mmm$, the single phase of which was observed at $x \geq 0.83$. The products at $x = 0.57$ and 0.7, therefore seem to be mixtures of the two solid solutions. Table 1 shows the lattice dimensions of a pseudotetrahedral cell, containing one triple-perovskite layer and one interlayer, in terms of a_T and c_T . The c_T value of the C222 phase was decreased with partial replacement of K^+ by Na^+ with a smaller ionic radius, because the value corresponds to the sum of the thickness of a triple perovskite layers and a gallery height of an alkaline metal layer (Fig. 1). By contrast, the a_T value, which should be determined by the size of the single perovskite unit, was almost constant irrespective of the Na content. At $x = 0.57$, a sudden increase of c_T and the change of space group from C222 to $I4/mmm$ took place simultaneously. Judging from a significant increase of hydration number (n), the structural change is due to the interlayer hydration. Assuming the random distribution of Na^+ in the interlayer space, its occupancy of about 50% seems to be needed to cause the interlayer hydration.

Fig. 3 exhibits the TG curves for $K_{1-x}Na_xCa_2Ta_3O_{10}$ measured in a dry gas mixture of 20% O_2 in N_2 . Small weight losses observed at $x < 0.3$ would be caused by desorption of physisorbed water. On the other hand, the samples at $x > 0.3$ were characterized by a large weight loss at 70–200 °C due to elimination of water from the interlayer. Clearly, the dehydration took place in two steps and the weight loss of each step became almost equivalent when x was close to the unity. A fully hydrated phase is therefore dehydrated via a half-filled intermediate phase to an anhydrous phase.

Fig. 4 shows the FT-IR spectra in the range of OH stretching mode (ν_{OH} , 3300–3500 cm^{-1}) and HOH bending mode (δ_{HOH} , 1600–1800 cm^{-1}). Essentially, normal modes of vibration in H_2O contain two OH stretching modes and one HOH bending mode. However, this is not the case because the hydrated $K_{1-x}Na_xCa_2Ta_3O_{10}$ ($0.57 \leq x \leq 1$) yielded sharp doublets at each region. The reason for such an extra infrared absorption is not clear at this stage, but one possibility is due to a hydrogen bonding not only between water molecules but also to lattice oxygen (O_L) of a TaO_6 octahedron forming H–O–H– O_L species in the interlayer.

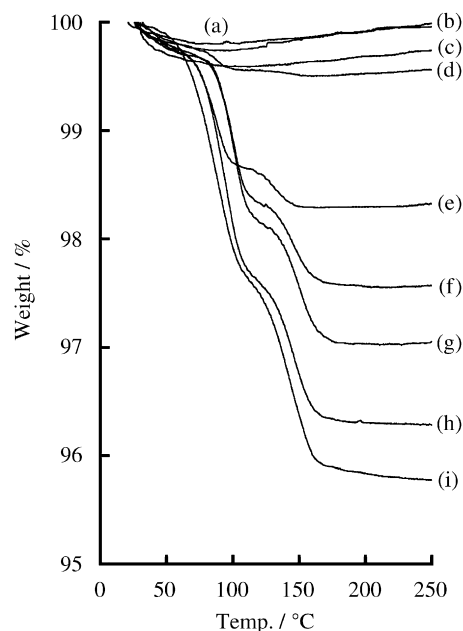


Fig. 3. TG curves of $K_{1-x}Na_xCa_2Ta_3O_{10} \cdot nH_2O$: (a) $x = 0$, (b) 0.09, (c) 0.22, (d) 0.30, (e) 0.57, (f) 0.70, (g) 0.83, (h) 0.91 and (i) 1.

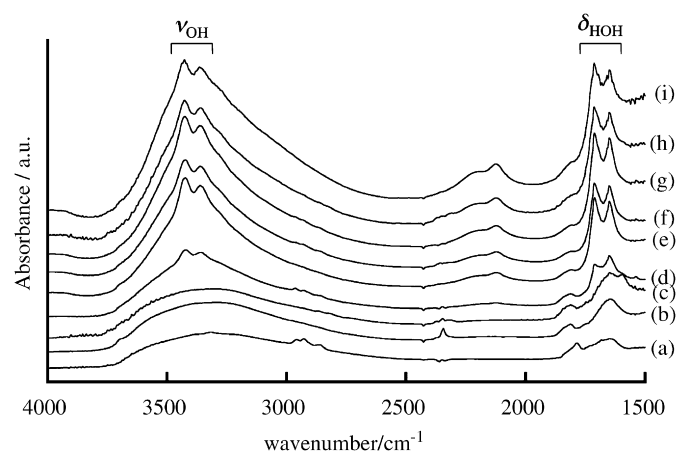


Fig. 4. FT-IR spectra of $K_{1-x}Na_xCa_2Ta_3O_{10} \cdot nH_2O$: (a) $x = 0$, (b) 0.09, (c) 0.22, (d) 0.30, (e) 0.57, (f) 0.70, (g) 0.83, (h) 0.91 and (i) 1.

3.3. $Li_{1-x}Na_xCa_2Ta_3O_{10} \cdot nH_2O$

$Li_{1-x}Na_xCa_2Ta_3O_{10}$ ($0 \leq x \leq 1$) was synthesized in a similar way by ion exchange at 400 °C using mixed molten nitrates ($LiNO_3$ – $NaNO_3$) with different ratios as shown in Table 2. Unlike the previous system, Na content (x) in the product was quite different from compositions of the melt, because the melting points of $LiNO_3$ (261 °C) and $NaNO_3$ (308 °C) are very different. Solids exchanged in mixed molten nitrates containing only 3 mol% $LiNO_3$ showed more than 99% Li in the interlayer as a result of selective incorporation. When the exchange was carried out at lower temperatures, however, solid products containing mixed alkali metals could not be obtained as a single phase. Therefore, we had to control the x value at extremely low $LiNO_3$ concentration (< 3 mol%) in the mixed molten nitrate at 400 °C, where x was increased with the composition of mixed molten nitrate.

Fig. 5 shows the XRD pattern of as exchanged $Li_{1-x}Na_xCa_2Ta_3O_{10}$. As is summarized in Table 2, the diffraction patterns were assigned to a tetragonal $I4/mmm$ space group except for $x = 0.54$,

Table 2
Composition and structure of $\text{Li}_{1-x}\text{Na}_x\text{Ca}_2\text{Ta}_3\text{O}_{10} \cdot n\text{H}_2\text{O}$

| Entry | Melt composition ^a | x | Space group | c_T/nm^b | a_T/nm^c | n^d |
|-------|-------------------------------|------|-------------|-------------------|-------------------|-------|
| a | 0 | 0 | $I4/mmm$ | 1.4217 | 0.3851 | 0 |
| b | 0.970 | 0.45 | $I4/mmm$ | 1.4122 | 0.3854 | 0.59 |
| c | 0.990 | 0.54 | $I4/mmm$ | 1.4162 | 0.3864 | 1.01 |
| d | 0.997 | 0.77 | $P4/mmm$ | 1.5233 | 0.3859 | |
| e | 0.999 | 0.85 | $I4/mmm$ | 1.6890 | 0.3860 | 1.82 |
| f | 1.000 | 1.00 | $I4/mmm$ | 1.6911 | 0.3862 | 1.91 |

^a $\text{NaNO}_3/(\text{NaNO}_3+\text{LiNO}_3)$.

^b d_{002} for $I4/mmm$, d_{001} for $P4/mmm$.

^c $2d_{200}$.

^d Hydration number.

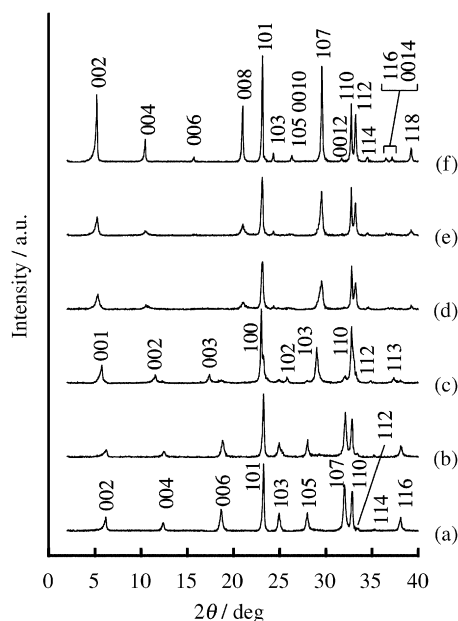


Fig. 5. XRD patterns of $\text{Li}_{1-x}\text{Na}_x\text{Ca}_2\text{Ta}_3\text{O}_{10} \cdot n\text{H}_2\text{O}$: (a) $x = 0$, (b) 0.45, (c) 0.54, (d) 0.77, (e) 0.85 and (f) 1.

where a primary phase having a $P4/mmm$ symmetry was observed. A significant shift of the (001) peaks to lower 2θ occurred at $x = 0.54$, suggesting the expansion of the interlayer distance (c_T) from 1.42 nm ($I4/mmm$) to 1.52 nm ($P4/mmm$) because of the accommodation of about 1 mol mol⁻¹ water into the interlayer. A further replacement by Na ($x \geq 0.77$) restored the original space group of $I4/mmm$, but the interlayer hydration close to $n = 2$ was achieved. A small increase of the interlayer distance at $x \geq 0.77$ can be explained by the larger ionic radius of Na^+ compared with Li^+ . The lattice constant, a_T , was kept almost constant for all the samples. These results are consistent with the structural change from an anhydrous phase ($x < 0.5$, $n \sim 0$) via a half-hydrated intermediate ($x \sim 0.5$, $n \sim 1$) and finally to fully hydrated phase ($x \sim 1.0$, $n \sim 2$).

As shown in Fig. 6, dehydration behavior measured by TG was very similar to that of $\text{K}_{1-x}\text{Na}_x\text{Ca}_2\text{Ta}_3\text{O}_{10}$ (Fig. 3). The fully hydrated phase exhibited a two-step weight loss, which is consistent with the dehydration process via half-filled intermediates. The hydration number increased monotonically with an increase of Na^+ content at $x \geq 0.45$. Fig. 7 shows the FT-IR spectra of $\text{Li}_{1-x}\text{Na}_x\text{Ca}_2\text{Ta}_3\text{O}_{10}$, which was also similar to that of $\text{K}_{1-x}\text{Na}_x\text{Ca}_2\text{Ta}_3\text{O}_{10}$. For $x \geq 0.45$, two doublets appeared at 3300–3500 and 1600–1800 cm^{-1} , indicating that interlayer hy-

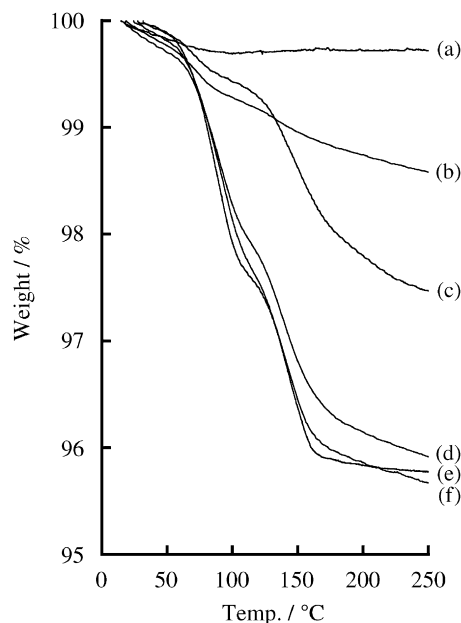


Fig. 6. TG curves of $\text{Li}_{1-x}\text{Na}_x\text{Ca}_2\text{Ta}_3\text{O}_{10} \cdot n\text{H}_2\text{O}$: (a) $x = 0$, (b) 0.45, (c) 0.54, (d) 0.77, (e) 0.85 and (f) 1.

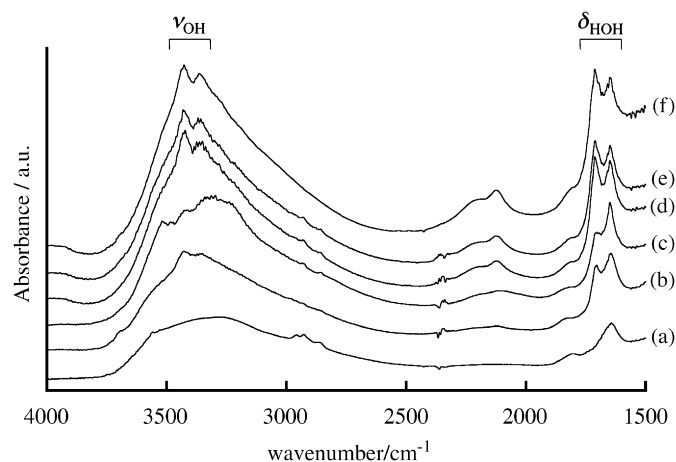


Fig. 7. FT-IR spectra of $\text{Li}_{1-x}\text{Na}_x\text{Ca}_2\text{Ta}_3\text{O}_{10} \cdot n\text{H}_2\text{O}$: (a) $x = 0$, (b) 0.45, (c) 0.54, (d) 0.77, (e) 0.85 and (f) 1.

dration possibly formed the strong interaction between waters and perovskite layers.

3.4. Relationship between interlayer hydration and photocatalytic activity

Finally, all the as-exchanged compounds were applied to photocatalytic water splitting under UV irradiation after loading 0.5 wt% Ni as a co-catalyst. In the preparation of Ni-loaded catalysts, the heating after impregnation of $\text{Ni}(\text{NO}_3)_2$ removed interlayer water from hydrated tantalates, but anhydrate phases thus formed could restore the hydrate phases on exposure to moisture/water at the ambient temperature. The optical band-gap energy of $A'_{1-x}\text{Na}_x\text{Ca}_2\text{Ta}_3\text{O}_{10}$ ($A' = \text{Li}$ and K) was almost the same in the range 4.2–4.3 eV, because the valence band and the conduction band consist commonly of $O2p$ and $\text{Ta}5d$, respectively [19]. Alkali metals do not contribute directly to the band-gap

excitation and subsequent transfer processes of photo-generated holes and electrons. The exchanged phases showed almost similar BET surface area ($\leq 5 \text{ m}^2 \text{ g}^{-1}$) and crystallite size (0.5–1 μm). The photocatalytic activity should therefore be free from microstructural effects.

All the 0.5 wt% Ni-loaded compounds exhibited steady-state evolution of H_2 and O_2 close to a stoichiometric ratio (2:1). Fig. 8 shows the rates of photocatalytic gas evolution and hydration number of $\text{K}_{1-x}\text{Na}_x\text{Ca}_2\text{Ta}_3\text{O}_{10} \cdot n\text{H}_2\text{O}$. Although the figure shows some scatter probably because of the loading of NiO co-catalysts was not uniform, the following trends are obtained. The activity was almost the same at $x < 0.3$, where anhydrous orthorhombic phases were formed. This indicates the partial substitution of Na for K does not affect the photocatalytic activity as can be expected from the electronic structure and microstructure as above mentioned. After the hydration occurred at $x \geq 0.3$, however, the activity was increased with the hydration number, giving rise to the maximum at $x = 1.0$. The result clearly supports that interlayer hydration is effective in photocatalytic activity of the present system.

Fig. 9 shows the rates of photocatalytic gas evolution and hydration number (n) of $\text{Li}_{1-x}\text{Na}_x\text{Ca}_2\text{Ta}_3\text{O}_{10} \cdot n\text{H}_2\text{O}$. The photocatalytic activity seemed to be constant when the Na content is not enough for the interlayer hydration ($x \leq 0.5$). The rates were then increased steeply to the highest values, 673 $\mu\text{mol H}_2 \text{ h}^{-1}$ and 310 $\mu\text{mol O}_2 \text{ h}^{-1}$, at $x = 0.77$. Interestingly, however, further substitution by Na decreased the activity in spite of incremental hydration number. It should also be noted that the activity can be enhanced by combining Na and Li in the interlayer space. This is quite different from the $\text{K}_{1-x}\text{Na}_x\text{Ca}_2\text{Ta}_3\text{O}_{10} \cdot n\text{H}_2\text{O}$ system, the activity of which increased monotonically with n .

These results of the photocatalytic water splitting of the present two systems clearly suggest that the interlayer hydration

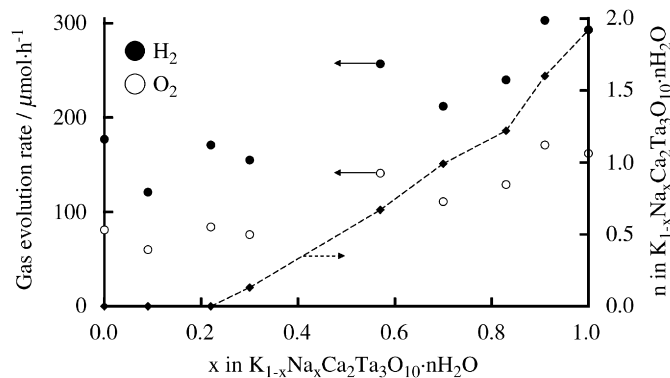


Fig. 8. Photocatalytic activity of $\text{K}_{1-x}\text{Na}_x\text{Ca}_2\text{Ta}_3\text{O}_{10} \cdot n\text{H}_2\text{O}$.

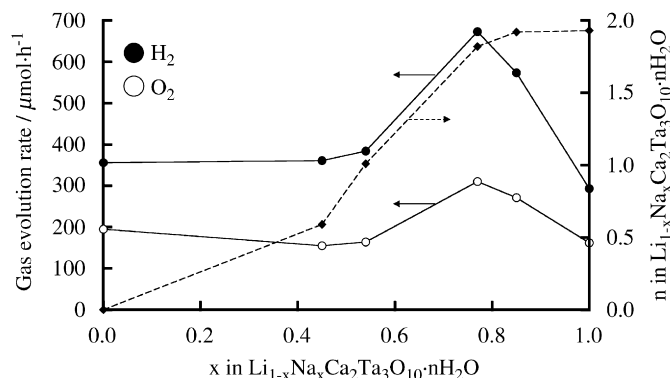
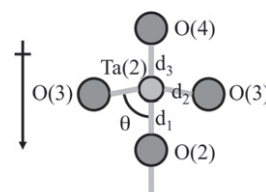


Fig. 9. Photocatalytic activity of $\text{Li}_{1-x}\text{Na}_x\text{Ca}_2\text{Ta}_3\text{O}_{10} \cdot n\text{H}_2\text{O}$.

plays a key role, but it is not the sole factor especially for the $\text{Li}_{1-x}\text{Na}_x\text{Ca}_2\text{Ta}_3\text{O}_{10}$ system. As was reported in our previous paper [20], the photocatalytic activity of $\text{LiCa}_2\text{Ta}_3\text{O}_{10}$ is highest among the series of $\text{A}'\text{Ca}_2\text{Ta}_3\text{O}_{10}$ ($\text{A}' = \text{Li, Na, K, Rb and Cs}$). This indicates that alkaline metals themselves affect the photocatalytic activity even though they do not affect microstructure and electronic structure of the layered tantalate. One plausible reason is that their effect is associated with the local structure of triple-perovskite layers. According to the work done by Inoue et al. [23,24], the photocatalytic activity may be correlated with the dipole moment of a metal-oxygen polyhedron. In case of the perovskite-related structure, the distortion of an octahedron would generate dipole moments, which lead to a local electric field useful for the electron-hole separation upon photoexcitation.

The dipole moment of the $\text{A}'\text{Ca}_2\text{Ta}_3\text{O}_{10}$ ($\text{A}' = \text{Li and Na}$) can be calculated using crystallographic data reported by Toda et al. [21,22]. As shown in Fig. 10, the triple perovskite layers of $\text{A}'\text{Ca}_2\text{Ta}_3\text{O}_{10}$ contains two types of octahedral TaO_6 . In contrast to the almost symmetric corner-shared $\text{Ta}(1)\text{O}_6$ in the center, $\text{Ta}(2)\text{O}_6$ in both side of the triple layer are highly distorted to yield the $\text{Ta}(2)\text{--O}(4)$ terminal bond very shorter than $\text{Ta}(2)\text{--O}(2)$ bridging bond and $\text{O}(2)\text{--Ta}(2)\text{--O}(3)$ angle smaller than 90° (Fig. 10). Owing to such axial distortion of apical oxygens and off-plane distortion of the equatorial oxygens, the position of the Ta^{5+} deviates from the center of the gravity to generate the dipole moment of $\text{Ta}(2)\text{O}_6$. The dipole moments of the terminal $\text{Ta}(2)\text{O}_6$ are 12.5 D ($\text{A}' = \text{Li}$) and 8.4 D ($\text{A}' = \text{Na}$), suggesting the higher distortion occurs when Li occupies the interlayer site. Although the structural parameters in the present $\text{Li}_{1-x}\text{Na}_x\text{Ca}_2\text{Ta}_3\text{O}_{10}$ system is not available at this moment, the bond length of $\text{Ta}(2)\text{--O}(4)$ can be estimated from the Raman frequency ascribable to the symmetric stretching mode of $\text{Ta}\text{--O}$ terminal bond in the region of $900\text{--}950 \text{ cm}^{-1}$ [25] as shown in Fig. 11. Upon replacing Li by Na, the peak at 943 cm^{-1} became less intense, whereas the peak at 930 cm^{-1} was intensified. This is consistent with a shorter $\text{Ta}(2)\text{--O}(4)$ terminal bond for the Li-rich phases having a highly distorted $\text{Ta}(2)\text{O}_6$ ($x \geq 0.77$), compared with the Na-rich phases ($x \leq 0.45$). The resulting distortion of the octahedral TaO_6 generates the internal electric fields due to the dipole moments, which would promote the separation of photogenerated holes/electrons. Such a geometric change and water accessible to the interlayer space are considered to yield a synergetic effect on the photocatalytic water splitting of the $\text{Li}_{1-x}\text{Na}_x\text{Ca}_2\text{Ta}_3\text{O}_{10}$ system.

Considering the structural advantage of $\text{LiCa}_2\text{Ta}_3\text{O}_{10}$ as a photocatalyst, its hydration is of great interest. Based on the thermodynamic consideration as above described, the difficulty for hydration of the Li phase is associated with the smallest interlayer distance, which would not allow water molecules to be intercalated. To overcome this problem, we have recently applied hydrothermal treatment and successfully synthesized an active



| A' | d_1 (Å) | d_2 (Å) | d_3 (Å) | θ (deg) | dipole moment (D) |
|-------------|-----------|-----------|-----------|----------------|-------------------|
| Li | 2.111 | 2.003 | 1.715 | 73.98 | 12.5 |
| Na | 2.372 | 1.953 | 1.806 | 81.22 | 8.4 |

Fig. 10. Dipole moment of octahedral $\text{Ta}(2)\text{O}_6$ in $\text{A}'\text{Ca}_2\text{Ta}_3\text{O}_{10}$ ($\text{A}' = \text{Li, Na}$).

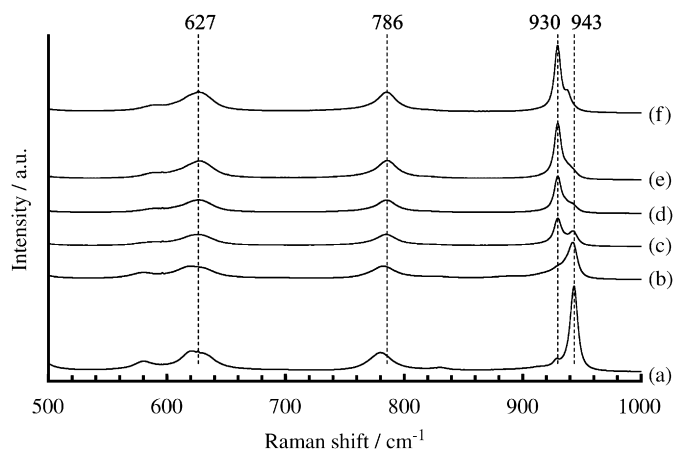


Fig. 11. Raman spectra of $\text{Li}_{1-x}\text{Na}_x\text{Ca}_2\text{Ta}_3\text{O}_{10}$: (a) $x = 0$, (b) 0.45, (c) 0.54, (d) 0.77, (e) 0.85 and (f) 1.

hydrated $\text{LiCa}_2\text{Ta}_3\text{O}_{10}$ [20]. The rates of gas evolution could be increased to $708 \mu\text{mol H}_2 \text{ h}^{-1}$ and $333 \mu\text{mol O}_2 \text{ h}^{-1}$, which are more than double of those for the anhydrous compound (0.5 wt% Ni loaded). The present study has demonstrated the partial replacement of Li by Na is an alternative way to hydrate the Li phase. The highest activity of $\text{Li}_{1-x}\text{Na}_x\text{Ca}_2\text{Ta}_3\text{O}_{10}$ ($x = 0.77$) is very close to those obtained for the hydrothermally treated Li phase.

4. Conclusion

$A'_{1-x}\text{Na}_x\text{Ca}_2\text{Ta}_3\text{O}_{10} \cdot n\text{H}_2\text{O}$ ($A' = \text{K}$ and Li) photocatalysts were synthesized by exchange in mixed molten nitrates. The replacement by Na caused the interlayer hydration, which is effective in enhancement of photocatalytic activity for water splitting under irradiation of UV light. The photocatalytic activity for $A' = \text{K}$ tends to increase with an increase of n . By contrast, the activity for $A' = \text{Li}$ showed the maximum at $x = 0.77$, indicating that not only

water molecules but Li ions in the interlayer space plays a key role in the overall water splitting reactions.

Acknowledgment

This work was financially supported by Core Research for Evolutional Science and Technology (CREST).

References

- [1] K. Domen, S. Naito, M. Soma, T. Ohnishi, K. Tamaru, *J. Chem. Soc. Chem. Commun.* (1980) 543.
- [2] K. Domen, S. Naito, T. Ohnishi, K. Tamaru, *Chem. Phys. Lett.* 92 (1982) 433.
- [3] K. Domen, A. Kudo, T. Ohnishi, *J. Catal.* 102 (1986) 92.
- [4] A. Kudo, A. Tanaka, K. Domen, K. Maruya, K. Aika, T. Ohnishi, *J. Catal.* 111 (1988) 67.
- [5] A. Kudo, K. Sayama, A. Tanaka, K. Asakura, K. Domen, K. Maruya, T. Onishi, *J. Catal.* 120 (1989) 337.
- [6] Y. Inoue, T. Kubokawa, K. Sato, *Chem. Commun.* (1990) 1298.
- [7] Y. Inoue, T. Niiyama, Y. Asai, Y. Sato, *Chem. Commun.* (1992) 579.
- [8] T. Takata, K. Shinohara, A. Tanaka, M. Hara, J.N. Kondo, K. Domen, *J. Photochem. Photobiol.* 106 (1997) 45.
- [9] T. Takata, Y. Furumi, K. Shinohara, A. Tanaka, M. Hara, J.N. Kondo, K. Domen, *Chem. Mater.* 9 (1997) 1063.
- [10] A. Kudo, H. Kato, *Chem. Lett.* (1997) 867.
- [11] K. Sayama, A. Tanaka, K. Domen, K. Maruya, T. Onishi, *J. Photochem. Photobiol. A: Chem.* 114 (1998) 125.
- [12] T. Ishihara, H. Nishiguchi, K. Fukamachi, T. Takita, *J. Phys. Chem. B* 103 (1999) 1.
- [13] M. Machida, J. Yabunaka, T. Kijima, *Chem. Commun.* (1999) 1939.
- [14] A. Kudo, H. Kato, S. Nakagawa, *J. Phys. Chem. B* 104 (2000) 571.
- [15] M. Machida, J. Yabunaka, T. Kijima, *Mater. Chem.* 12 (2000) 812.
- [16] H. Kato, A. Kudo, *J. Phys. Chem. B* 105 (2001) 4285.
- [17] C.T.K. Thaminimulla, T. Takata, M. Hara, J.N. Kondo, K. Domen, *J. Catal.* 196 (2001) 362.
- [18] H. Kato, K. Asakura, A. Kudo, *J. Am. Chem. Soc.* 126 (2003) 3082.
- [19] M. Machida, T. Mitsuyama, K. Ikeue, S. Matsushima, M. Arai, *J. Phys. Chem. B* 109 (2005) 7801.
- [20] T. Mitsuyama, A. Tsutsumi, T. Hata, K. Ikeue, M. Machida, *Bull. Chem. Soc. Jpn.* 81 (2008) 401.
- [21] K. Toda, K. Uematsu, M. Sato, *J. Ceram. Soc. Jpn.* 105 (1997) 482.
- [22] K. Toda, M. Sato, *J. Mater. Chem.* 6 (1996) 1067.
- [23] J. Sato, S. Saito, H. Nishiyama, Y. Inoue, *J. Photochem. Photobiol. A: Chem.* 148 (2002) 85.
- [24] J. Sato, H. Kobayashi, Y. Inoue, *J. Phys. Chem. B* 107 (2003) 7970.
- [25] J.M. Jehng, I.E. Wachs, *Chem. Mater.* 3 (1991) 100.